Astronomy & Astrophysics manuscript no. output
July 15, 2026

The building blocks of 3D models of barred galaxies

II. Spiral structures

M. Harsoula[1] and M. Katsanikas[1, 2]

[1]Research center for Astronomy and Applied Mathematics, Academy of Athens, Soranou Efessiou 4, 115 27 Athens, Greece
[2]School of Mathematics, University of Bristol, Fry Building, Woodland Road, Bristol, BS8 1UG, United Kingdom
e-mail: mharsoul@academyofathens.gr; mkatsan@academyofathens.gr;

Received ; accepted

ABSTRACT

We conducted an orbital study of Milky Way-like models of barred galaxies of three degrees of freedom in order to detect the orbits that support different structures of the galaxies, such as rings and spiral arms. We performed a parametric study focused on the strength of the bar's perturbation Q_f (22%-60% in forces), and we studied different energy levels through the use of 4D Poincaré surfaces of section (PSSs) of the 6D phase space. We used the method of apocentric sections for orbits with initial conditions above the unstable manifolds of the planar ($PL_{1,2}$) family (or Lyapunov orbits) or other unstable periodic orbits that have a small initial component on the z-axis. We conclude that in all models with different bar perturbation values, different morphological structures are supported by 3D sticky chaotic orbits at different energy levels, including the envelope of the bar, the outer rings of the R_1 type, and spiral arms. Ring structures are mostly supported for smaller values of the bar's perturbations (Q_f), while spiral arm structures are supported for larger values of Q_f. We found 4D hypersurfaces (in the 4D PSS) along which 3D chaotic orbits that support the galactic structures are sticky for very long times before escaping from the system. Finally we determined the stickiness time of these orbits using the time evolution of the finite time Lyapunov characteristic number.

Key words. Galaxies: kinematics and dynamics, Galaxies: spiral, Galaxies: structure

1. Introduction

The orbital dynamics of barred galaxies have been investigated extensively. It has been firmly established that both planar and three-dimensional regular orbits associated with the stable periodic x_1 family (Contopoulos and Papayannopoulos 1980) play a crucial role in maintaining the bar's morphology, both in face-on views and in edge-on projections (see e.g. Patsis et al. 2003, 2009; Patsis and Katsanikas 2014; Chaves-Velasquez et al. 2017). Regarding the creation of spiral arms in barred galaxies, the theory that has prevailed in recent years is the manifold theory by Voglis et al. 2006 and Romero-Gómez et al. 2006. This theory has been tested and confirmed by galactic models and N-body simulations in many papers (see Paper I for bibliography).

In the first paper of this series (Harsoula and Katsanikas 2025, hereafter Paper I), we presented the case of a small bar-induced perturbation ($Q_f \approx 12\%$ in forces) in a Milky Way-like barred galaxy rotating with a constant pattern speed of Ω_b = 45 km/s/kpc, which lies in the range of the values proposed for the Milky Way in Gerhard (2011) and in Sanders et al. (2019). We concluded that although there existed planar spiral structures on the configuration space made out of the apocentric manifolds of all the planar unstable periodic orbits outside corotation, these spiral paths are not populated by 3D sticky chaotic orbits, as they all quickly became diffused outwards along these paths. Therefore, in the model of Paper I we showed that 3D sticky chaotic orbits only support outer ring-like structures of the R_1 and R_1R_2' type (see Buta and Combes 1996) for extremely long times (hundreds and thousands of Hubble times) before escaping from the system.

We want to emphasise here that when referring to orbits in the configuration space, we use the conventional terminology of the dynamical astronomy literature, where '2D' and '3D' orbits denote trajectories embedded in two- and three-dimensional configuration spaces, respectively. This should not be confused with the dimensionality of geometric objects in the 4D Poincaré surface of section (PSS), where terms such as 2D manifolds and 3D hypersurfaces denote their intrinsic (topological) dimension.

In this paper we study galactic models of bar perturbation with values that range from $Q_f \approx 20\%$ to $Q_f \approx 60\%$ and conclude that as the bar's perturbation becomes greater, bar driven spiral structures are supported from 3D sticky chaotic orbits at ever greater distances. At the same time, we find that different structures can be supported at different energy levels in all cases of the bar's perturbation, including the envelope of the bar, outer ring structures of the R_1 type, and spiral arms.

We used the same approach as in Paper I; that is, we located the planar $PL_{1,2}$ orbits and calculated their unstable manifolds in the phase space. The $PL_{1,2}$ orbits (nomenclature follows Voglis et al. 2006a) are a family of unstable short-period orbits around the Lagrangian points $L_{1,2}$ (also called Lyapunov orbits), and they are found for energy levels (En) greater than $En_{L_{1,2}}$. We studied the behaviour of the 3D sticky chaotic orbits lying above these planar manifolds in the 4D PSS ($y, \dot{y}, z, \dot{z}$, for x=0 and $\dot{x} < 0$) of the corresponding 6D phase space of the system.

Article published by EDP Sciences, to be cited as https://doi.org/10.1051/0004-6361/202659797

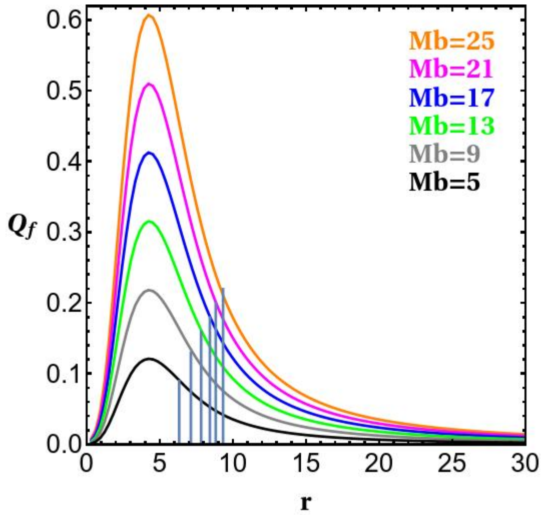

Fig. 1. Force perturbation of the bar (Q_f) as a function of the radius (r) for different values of the bar's mass (M_b). The maximum Q_f ranges from 12% up to 60%. The vertical lines give the positions of the corresponding Lagrangian points ($L_{1,2}$), which are located close to the bar's corotation

.

To facilitate visualisation of the 4D PSS, we used the method of colour and rotation (Patsis and Zachilas 1994). This method has been used to study various structures of the phase space of galactic-type Hamiltonian systems with three degrees of freedom (Katsanikas and Patsis 2011, Katsanikas et al. 2011a,b, Katsanikas et al. 2013, Katsanikas and Patsis 2022, Moges et al. 2024) and 4D symplectic maps (Zachilas et al. 2013, Agaoglou et al. 2021).

To study the stickiness time (or escape time) of 3D sticky chaotic orbits that behave as regular ones for a very long time, compared to the Hubble time, we used an important tool, namely, the time evolution of the finite time Lyapunov characteristic number ($FT-LCN$). We find that spiral structures on the configuration space can be supported by 3D chaotic orbits that present stickiness phenomena to some hypersurfaces resembling 2D manifolds (in the 4D PSS) and with the same foldings as the planar unstable manifolds lying underneath.

In our work for this paper, we used the same model as in Paper I, and we kept the same formalism. In Sect. 2 we give a quantitative estimation of the force strength of the bar. In Sect. 3 we explore the 6D phase space of the model with the help of 4D PSSs. We studied the 3D sticky chaotic orbits that support outer ring-like structures and spiral arms on the plane of rotation for different energy levels by plotting their apocentric sections on the plane of rotation. Finally we calculated the stickiness time (or escape time) of these sticky chaotic orbits. We present our conclusions in Sect. 4.

2. Force strength of the bar

In the present work we study the dependence of the galaxy structure on the parameter M_b of the bar's mass, which can also be attributed to the well-known parameter Q_f-force strength introduced by Laurikainen 2004 (see Paper I). In Fig. 1 we plot the value of Q_f as a function of the radius (r) for different values of the bar's mass ($M_b = 5, 9, 13, 17, 21, 25 \times 10^{10} M_{\odot}$). The maximum $Q_f(r)$ values correspond to perturbations of 12% up to 60%, covering almost the entire range of bar's perturbation of the corresponding values observed in real barred galaxies (see Laurikainen et al. 2004 and Buta et al. 2009). The vertical lines correspond to the position of the $L_{1,2}$ Lagrangian equilibrium points, which are located after the end of the bar and close to corotation. From this figure we observed a positive correlation between the length of the bar and the bar's strength, and this is something that has also been found in observations of barred galaxies (Gadotti 2011, Guo et al. 2019). Moreover, it has also been shown in simulations of barred galaxies that bars grow stronger in time by becoming longer as a result of angular momentum exchange between the inner and outer parts of galaxies (Athanassoula and Misiriotis 2002).

3. Exploration of the phase space

3.1. Locating the Lagrangian points L_1, L_2

We fixed the pattern speed of the bar to $\Omega_b = 45$ km/s/kpc in real units and $\Omega_b = 0.217$ in the units of the system. The procedure for locating the unstable Lagrangian points $L_{1,2}$ is described in Paper I, and the solutions were found in Cartesian coordinates $(x_{L_{1,2}}, y_{L_{1,2}}, z_{L_{1,2}}, p_{x_{L_{1,2}}}, p_{y_{L_{1,2}}}, p_{z_{L_{1,2}}})$. The orientation of the main axis of the bar on the plane of rotation is along the y-axis with respect to the rotating frame of reference. The $y_{L_{1,2}}$ coordinate, which is located after the end of the bar and close to corotation, is shown in Fig. 1 for the different models we studied.

The ratio R of the corotation radius (which is close to the Lagrangian points $L_{1,2}$) to the length of the bar (taken as equal to its major axis, $a = 5.25$; see Paper I) can be used as a tool to distinguish between fast and slow bars. Ultrafast bars have $R < 1.0$, fast bars have $1.0 < R < 1.4$, and slow bars have $R > 1.4$.

According to the aforementioned definition, the models we studied (distinguished by the different parameter of the bar's mass, M_b) can be separated into fast bars for $M_b = 5$ and 9, with $R = 1.2$ and $R = 1.35$, respectively, and slow bars for $M_b = 13, 17, 21$, and 25, with $R = 1.48$, $R = 1.6$, $R = 1.68$, and $R = 1.77$, respectively. This rough separation of weak-fast bars from strong-slow bars is consistent with the findings of Géron et al. (2023), as the authors concluded from observations of barred galaxies that strong bars tend to have lower bar pattern speeds.

3.2. 2D Poincaré surfaces of section

We studied the 2D PSSs of the planar orbits in order to detect the stickiness phenomena of planar chaotic orbits along unstable manifolds of unstable periodic orbits before extending our study to 3D sticky chaotic orbits. In the foundational studies of Perry and Wiggins 1994 and Morbidelli and Giorgilli 1995, the authors found that the escape times of chaotic orbits outside the borders of the islands of stability (regular motion) are superexponentially large. Since then, there have been many other works that adopted the term 'stickiness of chaotic orbits' to describe the phenomenon related to the extremely long times of escape. Studies in mappings and Hamiltonian systems of two degrees of freedom and three degrees of freedom have shown that chaotic orbits follow the paths and the folding of unstable invariant manifolds of unstable periodic orbits and of higher-dimensional transport structures in phase space, thus excessively delaying their diffusion outwards (Contopoulos and Harsoula 2008, 2010a, 2010b, and references within; Katsanikas, Patsis, and Contopoulos 2013; Contopoulos and Harsoula 2013; Wiggins et al. 2025).

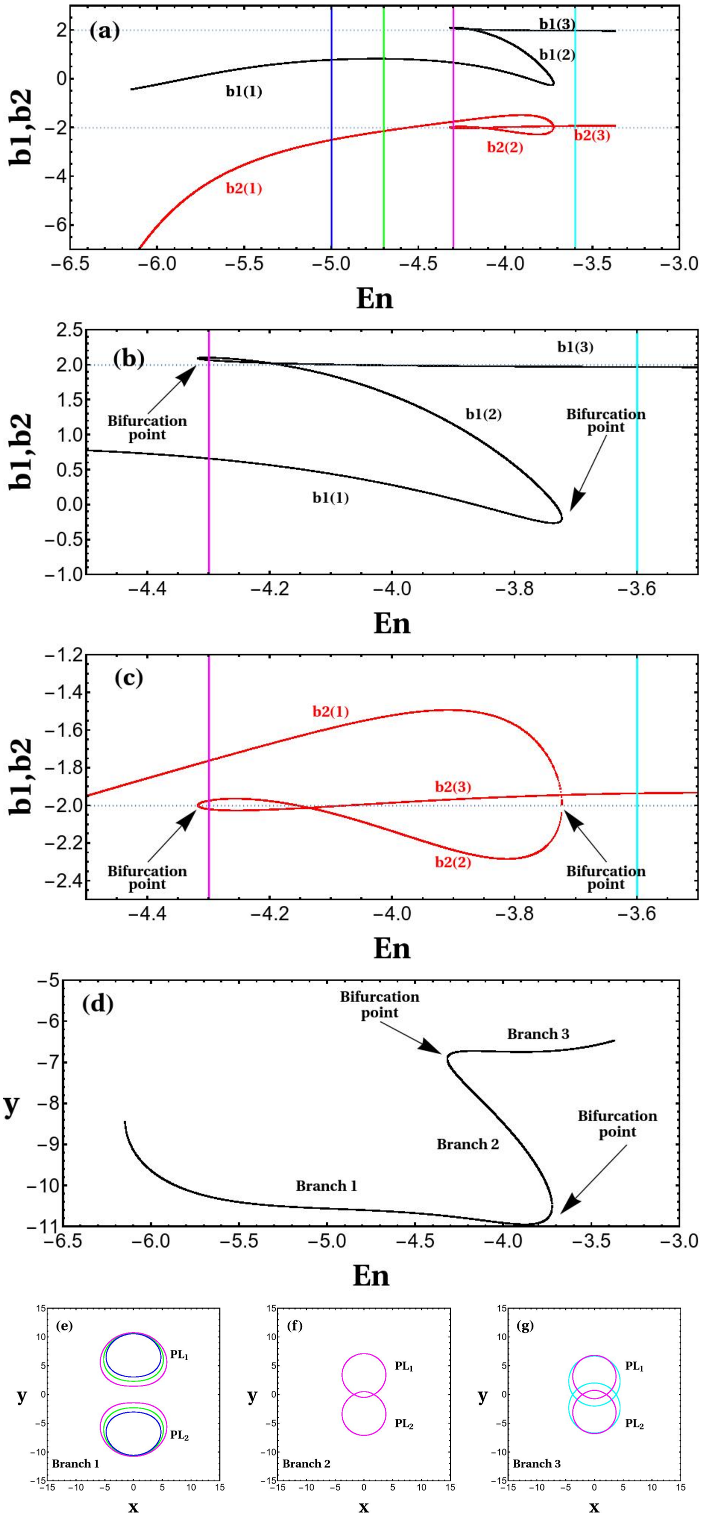

Fig. 2. (a) Stability indices, $b1, b2$, of the planar $PL_{1,2}$ orbit (branch 1, branch 2 and branch 3) as functions of the energy En, for bar's mass M_b = 17. The vertical stability index, $b1$, (black) corresponds to the stability of planar periodic orbits with respect to perturbations perpendicular to the orbital plane, while the planar stability index, $b2$, (red) corresponds to the stability with respect to perturbations on the orbital plane. The four vertical lines correspond to the energy levels at which we investigated the phase space. (b) and (c) A zoom of Fig. 2a showing the bifurcation points joining the branches 1 and 2 as well as the branches 2 and 3. (d) Characteristics of the three planar branches of the $PL_{1,2}$ family that are joined and disappear at the bifurcation points. Branch 1 (e), branch 2 (f) and branch 3 (g) planar $PL_{1,2}$ orbits plotted with the same colour as the corresponding energies (vertical lines) in Fig. 2a.

The Hamiltonian (or energy En) of the system, which rotates around the z-axis with an angular velocity (pattern speed) of Ω_b = 45 km/s/kpc, can be written in Cartesian coordinates in the rotating frame of reference in the form

$$En = (\frac{\dot{x}^2}{2} + \frac{\dot{y}^2}{2} + \frac{\dot{z}^2}{2}) + V(x, y, z) - \frac{1}{2}\Omega_b^2(x^2 + y^2), \tag{1}$$

where $V(x, y, z)$ is the sum of the axisymmetric and the bar potential (see Paper I).

We located the planar $PL_{1,2}$ family of orbits (or Lyapunov orbits) for energy levels (or equivalently Jacobi integrals) above $En_{L_{1,2}}$, and we studied their linear stability. Using the variational equations and considering small deviations from the initial conditions (y_{PL_1}, $\dot{y_{PL_1}}$, x_{PL_1} = 0, $\dot{x_{PL_1}}$ < 0), we studied their stability indices $b1, b2$ (for more details, see Appendix A of Paper I) as functions of the energy level En for a bar's perturbation M_b = 17 (corresponding to Q_f=40% perturbation in forces). This is a rather representative value of the bar's strength, and it corresponds to a strong slow bar (with R = 1.6). In recent studies of observations of samples of a sufficient number of barred galaxies, authors have concluded that the majority of them possess a strong and slow bar (Géron et al. 2023, Mengistu et al. 2026) .

In Fig. 2a we plot the stability indices as functions of the energy ($b1, 2 = f(En)$). The periodic orbit is a) stable if $\mid b1 \mid < 2$ and $\mid b2 \mid < 2$; b) simply unstable if $\mid b1 \mid < 2$ and $\mid b2 \mid > 2$ or $\mid b1 \mid > 2$ and $\mid b2 \mid < 2$; c) double unstable if $\mid b1 \mid > 2$ and $\mid b2 \mid > 2$; and d) complex unstable if $b1$ and $b2$ are complex numbers.

The vertical stability index $b1$ corresponds to the stability of planar periodic orbits with respect to perturbations perpendicular to the orbital plane, while the planar stability index $b2$ corresponds to the stability with respect to perturbations on the orbital plane. The four vertical lines correspond to the energy levels at which we investigated the phase space.

From Fig. 2a, we observed that there is a range of energies for which three different branches of $PL_{1,2}$ orbits coexist: branch 1, branch 2, and branch 3. As a consequence, there are two saddle-node bifurcation points, as can be seen in Figs. 2b,c, between branch 1 and branch 2 on the right and between branch 2 and branch 3 on the left. In Fig. 2d we plot the characteristics ($y = f(En)$) of all the branches of the $PL_{1,2}$ family of orbits, where the bifurcation points correspond to a local minimum or a local maximum of the y-coordinate. Finally, in Figs. 2e,f,g we plot the orbits that correspond to the different branches of the $PL_{1,2}$ family in the plane of rotation ($x - y$). The colours correspond to the energies denoted in Fig. 2a.

In Fig. 3 we plot the 2D PSS of the planar orbits, for M_b = 17, for the four energy levels denoted in Fig. 2a, i.e. $En = -3.6$ in Fig. 3a, $En = -4.3$ in Fig. 3b, $En = -4.7$ in Fig. 3c, and $En = -5.0$ in Fig. 3d. These energy levels are above the energy of the unstable Lagrangian equilibrium points $L_{1,2}$, which for this model is $En_{L_{1,2}} = -6.147$. The $PL_{1,2}$ family of orbits exist above $En_{L_{1,2}}$ (see Fig. 2a). In this figure only the branches of the PL_2 family are plotted (the PL_1 family is found for positive values of the y coordinate), where branch 1 of PL_2 is referred to in the figure as PL_2, branch 2 as PL_2', and branch 3 as PL_2''. The three branches of the PL_2 family coexist only in Fig. 3b (see Fig. 2). In Figs. 3c,d only branch 1 of the PL_2 family exists, which is unstable and located inside the chaotic region just outside the last Kolmogorov-Arnold-Moser (KAM) curve of the regular motion. Red curves in these figures are the unstable manifolds emanating from the PL_2 family. In Fig. 3b all the branches of the PL_2 family are located inside the last KAM of regular motion. In this case, red curves correspond to the unstable manifolds of an unstable

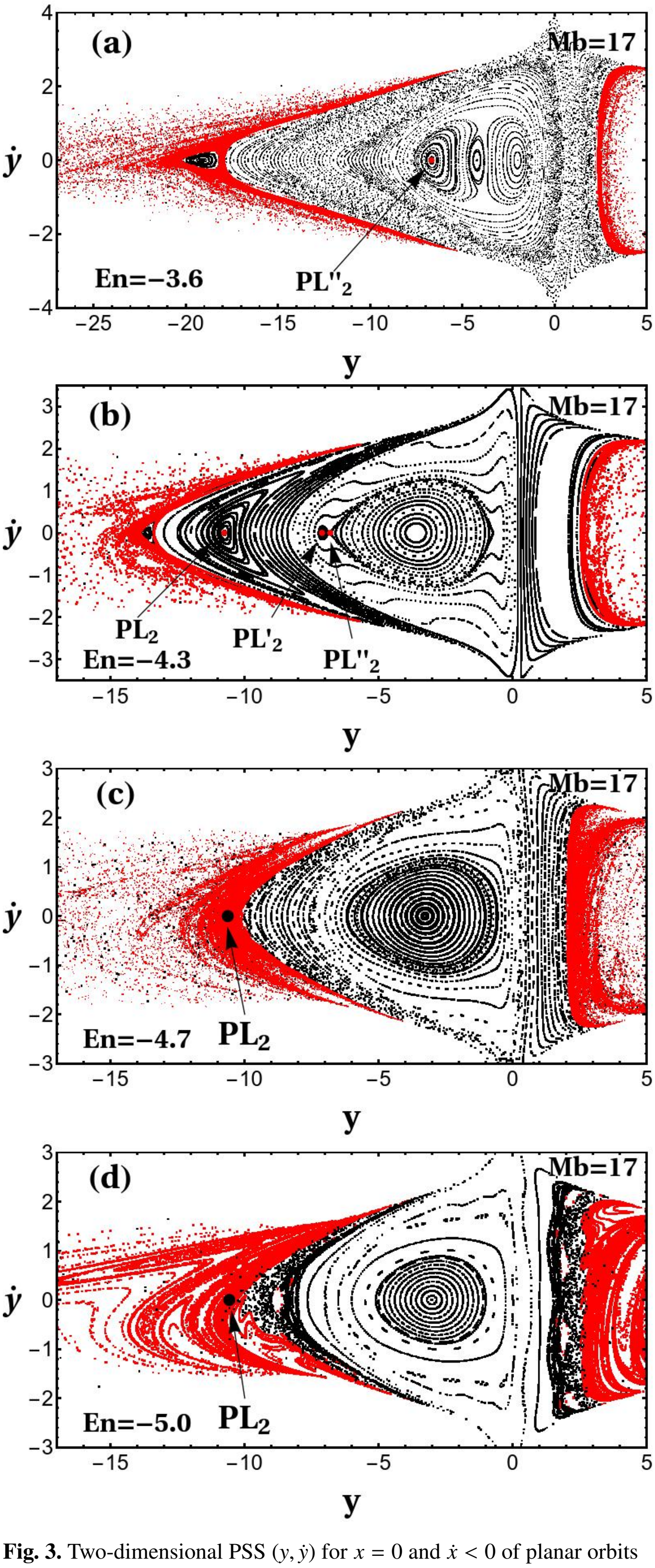

Fig. 3. Two-dimensional PSS $(y, \dot{y})$ for $x = 0$ and $\dot{x} < 0$ of planar orbits for four different energy levels: (a) En = 3.6, (b) En = -4.3, (c) En = -4.7, and (d) En =-5.0 , for $M_b = 17$. With red, we plot the unstable manifolds of the planar PL_2 orbit in (c) and (d), while in (a) and (b) we plot the unstable manifolds of the unstable periodic orbits just outside the last KAM curve of the regular motion.

periodic orbit just outside the last KAM curve. We emphasise here that all the unstable manifolds of the unstable periodic orbits, inside the chaotic region outside the last KAM curve, are parallel to each other and form the paths along which planar chaotic orbits will evolve through time and manifest the stickiness phenomena. Finally, in Fig. 3a only branch 3 of the PL_2 family exists, which is stable and well inside the region of regular motion. The red curves again correspond to unstable manifolds of planar unstable periodic orbits just outside the last KAM curve of the region of regular motion.

To study the behaviour of 3D sticky chaotic orbits, we took the initial conditions along these red curves of the unstable manifolds of Fig. 3 and gave them a small initial z component. Then we integrated these orbits for times comparable to the Hubble time and studied the structures that they support in the configuration space of the galaxy and the speed of their diffusion outwards. For this study we used 4D PSSs.

3.3. 4D Poincaré surfaces of section

We explored the 6D phase space for the same energy levels as in Fig. 3 in order to study the behaviour of the 3D sticky chaotic orbits. If we fix the initial values $(y_0, \dot{y_0}, z_0, \dot{z_0})$ of an orbit in the 4D PSS of the 6D phase space to $x_0 = 0$, the value of the coordinate $\dot{x_0}$ (velocity in the rotating frame) can be calculated for a specific energy (En) through Eq. (1):

$$\dot{x_0} = \pm\sqrt{2(En - V(x_0, y_0, z_0)) - \dot{y_0}^2 - \dot{z_0}^2 + \Omega_b^2(x_0^2 + y_0^2)}. \qquad (2)$$

We chose the negative solution of $\dot{x_0}$ in Eq. (2) for $y_0 < 0$, which is compatible with the direction of rotation of the orbits outside corotation in the rotating frame of reference.

In Fig. 4 we plot the 3D projection $(y,\ \dot{y},\ z)$ of the 4D PSS for the same energy levels and bar perturbation as in Fig. 3. In black we plot the 2D PSS ($y, \dot{y}$, for $x = 0$ and $\dot{x} < 0$) of the planar orbits that stay continuously on the x-y plane of rotation on the configuration space, and in green are the 3D sticky chaotic orbits (on the x-y-z configuration space) with initial conditions along and above the planar unstable invariant manifolds of unstable periodic orbits (red curves of Fig. 3), which have a small initial z-component (z_0=0.02 kpc).

In Figs. 4c and 4d we integrate sticky chaotic orbits (green points) with initial conditions along and above the unstable manifolds of the planar PL_2 family and that have a small initial z-component (z_0=0.02). In fact, although this is a rather small initial z value, for a better graphical representation of the results, we tested values up to z_0=0.3-0.7kpc (depending on the energy level), which correspond to the limits of the thickness of a Galactic disc, and we found the same behaviour (see for example Bland-Hawthorn and Gerhard 2016 for the disk thickness of the Milky Way.) We observed that although these chaotic orbits could escape through the z-component, they remain located above these manifolds for a long time before escaping from the system (through an Arnold web). In other words they exhibit stickiness phenomena in three-dimensional hypersurfaces for some time by having a regular orbit behaviour. The same is true in Figs. 4a and 4b, although the different branches of the planar PL_2 family are stable or unstable, but found inside the region of the regular motion. The 3D sticky chaotic orbits (green) here have initial conditions along and above the unstable manifolds of unstable periodic orbits just outside the region of the regular motion. Here again they present a sticky behaviour for a long time before diffusing outside of the system. For all the energy levels of Fig. 4, we checked all possible 3D projections of the 4D PSS $(y, \dot{y}, z, \dot{z})$ and concluded that the sticky chaotic orbits are in all cases restricted in finite volumes inside a radius of 30 kpc for times comparable to the Hubble time.

In Fig. 5 we give the percentage of sticky chaotic orbits having initial conditions above the unstable manifolds of Fig. 3 (red points) that stay located inside a radius of $r = 30$kpc when integrated (green points of Fig. 4) as a function of time (in units of Hubble time). We conclude that for the energy levels $En = -3.6, -4.3$, and -4.7, the stickiness time is greater than a Hubble time, while for the energy level $En = -5.0$, there still remains a great number of trapped orbits after a Hubble time, although orbits escape faster from the system.

In Fig. 6, we show a magnification of Fig. 4d in the 4D PSS ($y, \dot{y}, z, \dot{z}$; where the $\dot{z}$ coordinate is in the range $-0.025 < \dot{z} < 0.025$, in velocity units; see Paper I). In the figure, we have taken more dense initial conditions above the unstable manifold of the planar PL_2 orbit and integrated the orbits for a number of iterations corresponding to approximately a Hubble time. It is clear that these initial conditions correspond to 3D chaotic orbits that are sticky to a hypersurface that follows the foldings of the planar manifold. This hypersurface probably corresponds to a 3D manifold in the 4D PSS. From this figure it is clear how important the stickiness phenomenon of chaotic orbits is along invariant manifolds in the 2D and 4D phase space. In fact, the study of this hypersurface will be the subject of a future study. In Fig. 7 we plot the projection of the coloured 4D surface of Fig. 6 on the $(y, \dot{y})$ PSS. We observed that the projection itself follows the path of the 2D unstable manifold of the plane PL_2 family, which means that the foldings of the manifold stay unchanged in the 3D projection of the 4D PSS $(y, \dot{y}, z)$ of Fig. 6.

On the other hand, if we take the initial conditions along and above the KAM curves inside the regular motion of the planar orbits (with an initial small z-component, i.e. z_0=0.02) and integrate the orbits, we observe a different behaviour. In Fig. 8 we plot the time evolution of a 3D sticky chaotic orbit in the 4D PSS $(y, \dot{y}, z, \dot{z})$ that has initial conditions above the borders of the regular motion of planar orbits. The colour bar on the left indicates the gradient of the $\dot{z}$ component (the minimum value of $\dot{z}$ corresponds to zero and the maximum to one). In black, the 2D PSS of the planer orbits is plotted. Figure 8a corresponds to the first 2300 iterations (corresponding to approximately 14 Hubble times) showing a regular orbit behaviour. This orbit was then integrated for another 7700 iterations (Fig. 8b) to exhibit its chaotic behaviour, during which it diffused inwards close to the centre of the galaxy and spread over a larger volume. Finally in Fig. 8c, we plot the same orbit for another 16000 iterations, where it has uniformly covered this larger volume towards the centre of the galaxy and begun to spread outwards and escape from the system.

In Fig. 9 we plot the time evolution of the $FT - LCN$ of the orbit of Fig. 8 given by the relation $FT - LCN = \frac{1}{t} ln \frac{w(t)}{w(0)}$, where $w(0)$ is an initial deviation vector of the orbit and $w(t)$ is the deviation vector after a time t (see Appendix B in Paper I for details). More sophisticated chaos indicators, such as the fast Lyapunov indicator (FLI; Froeschlé 1997), MEGNO (Cincotta and Simó 2000), and SALI or GALI (Skokos 2001, Skokos et al. 2007), can indeed provide a more detailed characterisation of chaotic transport and escape mechanisms in higher-dimensional Hamiltonian systems. However, in the present work our main goal is not to perform a detailed mapping of the Arnold web but rather to estimate the characteristic trapping (stickiness) times of chaotic trajectories that support galactic morphological structures. For this purpose, the FT-LCN provides a sufficiently robust

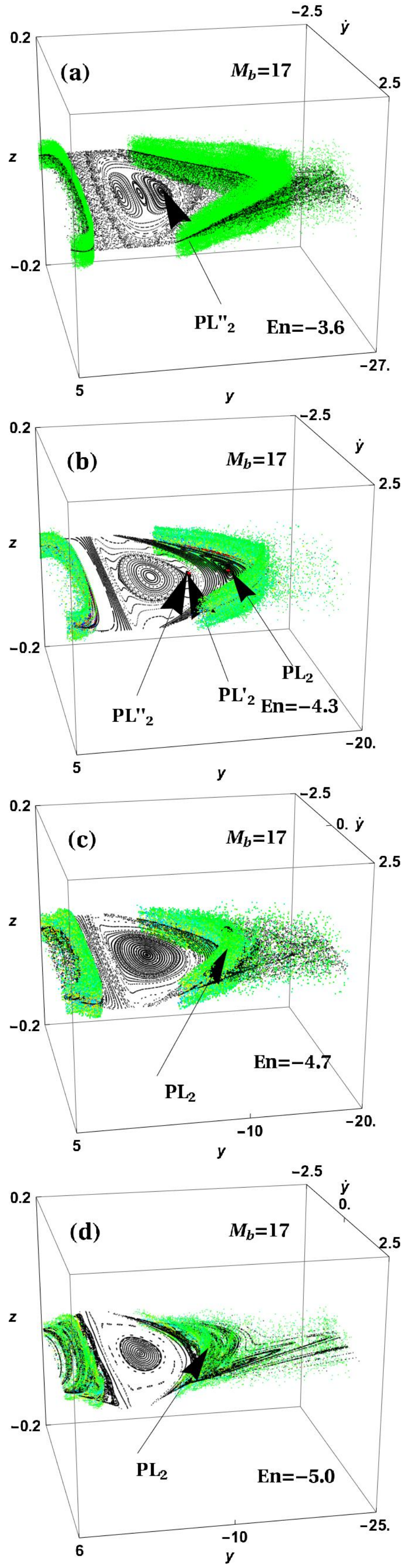

Fig. 4. Three-dimensional PSS $(y, \dot{y}, z)$ projection of the 4D PSS $(y, \dot{y}, z, \dot{z})$ for $x = 0$ and $\dot{x} < 0$ for energy levels (a) $En = 3.6$, (b) $En = 4.3$, (c) $En = 4.7$, and (d) $En = 5.0$ for $M_b = 17$. In Black we plot the 2D PSS of planar orbits. The 3D sticky chaotic orbits above the planar unstable manifold of the PL_2 family in (c) and (d) or of unstable periodic orbits just outside the last KAM curve of the regular motion in (a) and (b) (green points) remain located there for a very long time before escaping from the system.

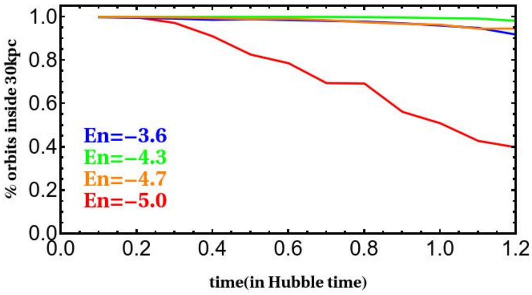

Fig. 5. Percentage of sticky chaotic orbits (green points in Fig. 4) that stay located inside the radius of $r = 30$ kpc as a function of time (in Hubble time units) for the four energy levels of Fig. 4.

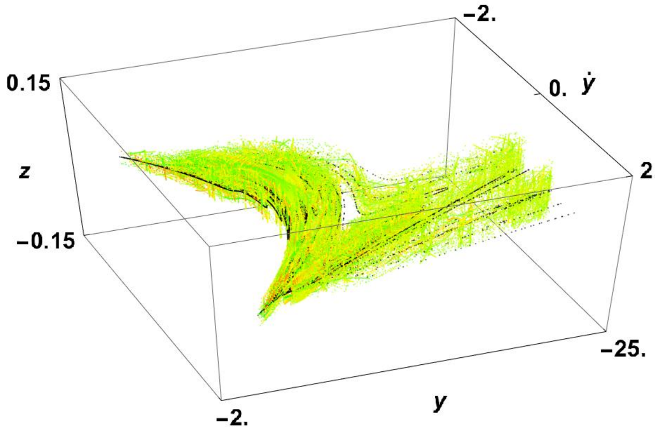

Fig. 6. Magnification of Fig. 4d with more dense initial conditions above the unstable manifold of the planar PL_2 orbit. The $\dot{z}$ coordinate is in the range $-0.025 < \dot{z} < 0.025$, in velocity units and is shown by a smooth colour gradient. The initial conditions correspond to 3D chaotic orbits that are sticky to a hypersurface that follows the foldings of the planar 2D manifold in the 3D PSS.

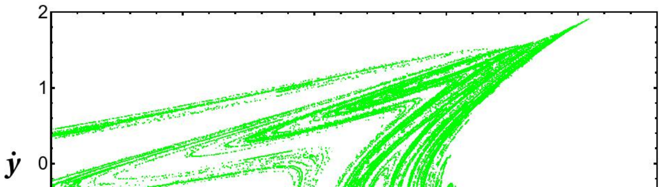

Fig. 7. Projection of the coloured 4D surface of Fig. 6 on the $(y, \dot{y})$ PSS, which follows the path of the 2D unstable manifold of the plane PL_2 family.

and physically transparent indicator, especially when combined with the corresponding study of the 4D PSS. The first decreasing part of the curve in Fig. 9 corresponds to the time interval during which the orbit exhibits a regular behaviour (see Fig. 8a). Later, there is an abrupt increase that corresponds to the time interval of Fig. 8b, where the orbit exhibits chaotic behaviour, becoming diffused inwards in a much larger volume. Finally, the $FT-LCN$ seems to converge at a constant positive value during the time interval of Fig. 8c, where the orbit has uniformly covered this larger volume towards the centre of the galaxy. The limit of FT-LCN for $t \to \infty$ is the well-known Lyapunov characteristic number. However, after this time interval, the calculations of the $FT-LCN$ were ceased because the orbit escapes to large distances from the system.

We also note that alternative approaches for quantifying chaotic transport and diffusion, such as Shannon entropy (Cincotta and Giordano 2023), Tsallis entropy (Tsallis 1988), and related entropy-based diagnostics, have been proposed in the literature. These methods provide complementary statistical descriptions of diffusion processes. However, the scope of the present work is mainly on the geometric and dynamical study of the phase-space structures based the 4D PSS and the $FT-LCN$, which allowed us to directly follow the confinement and escape of chaotic orbits in phase space.

In order to understand the limitations of the motion of 3D chaotic orbits in the 4D PSS ($y, \dot{y}, z, \dot{z}$, for $x = 0$), we plotted the surface of zero velocity (SZV). This corresponds to the boundary of the energetically allowed region for the 3D projection $(y, \dot{y}, z)$ of the 4D PSS, and it is calculated from Eq. (1) for $x = \dot{x} = \dot{z} = 0$. In Fig. 10 we plot the SZV superimposed on Figs. 8c, 4d for energy $En = -5.0$ and $M_b = 17$. We observed that the region inside corotation can communicate with the region outside corotation. Nevertheless, although the 3D yellow chaotic orbit is only partly limited by the SZV (with initial conditions inside corotation), it stays located in a specific region inside corotation and escapes from the system after hundreds of Hubble time. The 3D green chaotic orbit, on the other hand, is not at all bounded by the SZV but exhibits stickiness along a hypersurface (see Fig. 6) above the unstable manifold of the planar PL_2 family. From this figure we concluded that there must exist some other hypersurfaces in the 4D PSS (apart from the SZV) that cause the stickiness phenomena of the 3D chaotic orbits. In fact, this is the subject of a future study. We emphasise here that for values of the energy (En) smaller than the one corresponding to the Lagrangian points ($En_{L_{1,2}}$), the part of the SZV inside corotation is closed. As a consequence, the 3D orbits with initial conditions inside corotation cannot escape from this region and mostly support the structure of the bar.

3.4. Apocentric sections

In this section we focus on the effect of the 3D sticky chaotic orbits (studied in the previous section in the 4D PSS) on the morphological structures of the galaxy in the configuration space (e.g. rings and spiral arms). The well-known method to study this effect involves plotting the 'apocentric manifolds' (Voglis et al. 2006a, Tsoutsis et al. 2008, 2009, Harsoula and Katsanikas 2025). For this purpose, we took as the initial conditions ($y_0, z_0, \dot{y_0}, \dot{z_0}$, with x_0=0 and $\dot{x_0}$ derived from Eq. 2) the green points of Fig. 4, which correspond to 3D chaotic orbits lying above (with a small initial z-component, $z_0 = 0.02$) the unstable manifolds of the planar PL_2 or other unstable periodic orbits inside the chaotic region near the border of regular motion. We then integrated these chaotic orbits for a time comparable to the Hubble time and plotted only the apocentres of the projections in the x-y configuration space. We call these points 'apocentric sections' and not 'apocentric manifolds' because these initial conditions are not found along the planar unstable manifolds.

In Paper I, where we studied the case of a small bar perturbation with $M_b = 5$ (only 12% in forces), we concluded that although the planar apocentric manifolds of planar unstable periodic orbits form a path with spiral structures, these paths are not populated by 3D sticky chaotic orbits. The latter orbits support ring structures of the R_1 or R_1R_2' type for hundreds or thou-

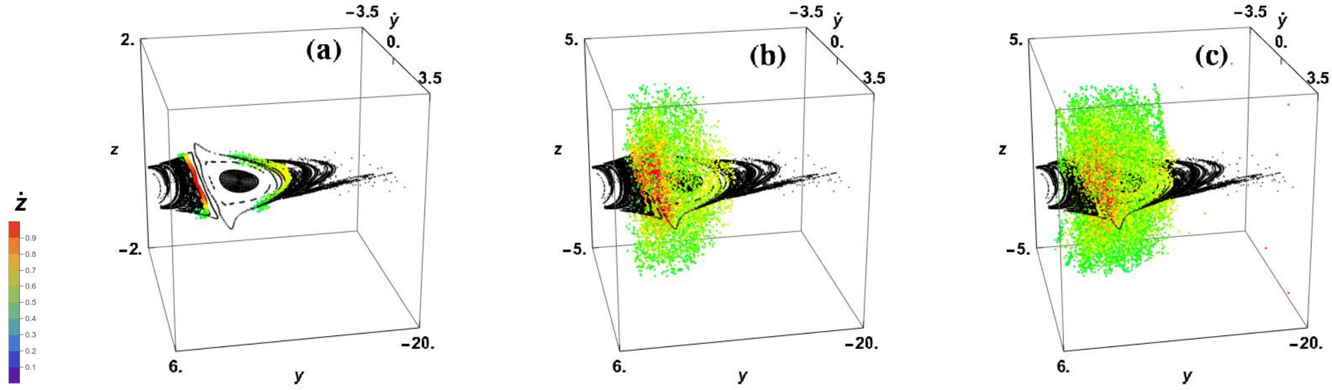

Fig. 8. Four-dimensional PSS $(y, \dot{y}, z, \dot{z})$ of a 3D sticky chaotic orbit (coloured points) that is trapped in smaller radii for a very long time before finally escaping from the system. The gradient of the colour indicates the $\dot{z}$ component, according to the colour bar on the left; the minimum $\dot{z}$ corresponds to zero and the maximum $\dot{z}$ to one. The bar's mass is $M_b = 17$, and the corresponding energy is $En = -5.0$. (a) Plot of the orbit for the first 2300 iterations. The orbit presents a regular behaviour. (b) Plot of the orbit for the next 7700 iterations. The orbit spreads in a larger volume towards the centre of the galaxy. (c) Plot of the orbit for the next 16000 iterations. After this extremely long time, the orbit escapes from the system.

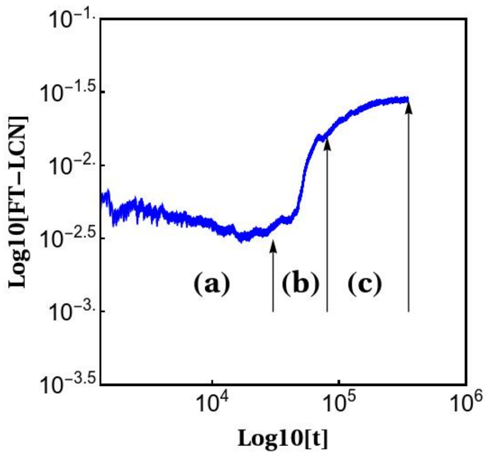

Fig. 9. Time evolution of the $FT-LCN$ of the 3D sticky chaotic orbit of Fig. 8 in a log-log scale. The first part of the curve corresponds to Fig. 8a and decreases as function of time, indicating a regular behaviour. The part of the curve corresponding to Fig. 8b shows an abrupt increase, indicating a chaotic behaviour. Finally, the curve converges to a specific LCN before the orbit escapes from the system.

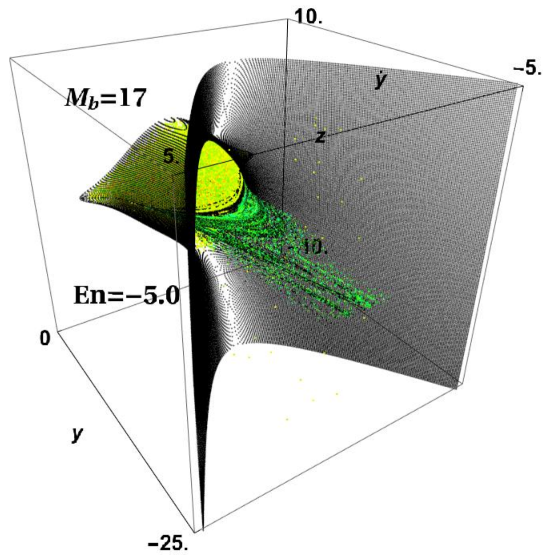

Fig. 10. Three-dimensional PSS $(y, \dot{y}, z)$ of the 3D sticky chaotic orbits of Figs. 8c and 4d superimposed on the SZV for energy $En = -5.0$ and $M_b = 17$. The 3D yellow orbit is partly limited by the SZV inside corotation and escapes after a very long time of integration, while the 3D green chaotic orbit is not bound by the SZV but exhibits stickiness phenomena in a 3D hypersurface along and above the unstable manifold of the planar PL_2 family.

sands of Hubble times, but they later quickly become diffused outwards, escaping from the system without supporting any spiral arms.

In Fig. 11 the apocentric sections of the 3D sticky chaotic orbits of Fig. 4 are plotted for a value of the bar's perturbation, $M_b = 17$ (corresponding to a force perturbation of approximately $Q_f = 40\%$), in the configuration space x-y for different energy levels. Although these orbits could escape through the third dimension (z-component), they stay and support ring and spiral structures for long enough times compared to the Hubble time. We observed that different morphological structures are supported in each energy level, namely the envelope of the bar, outer ring, and bar-driven spiral structures.

In Fig. 12 we plot the apocentric sections for different values of the bar's perturbation (M_b=9-25) and for different levels of the energy (En). We observed again that different morphological structures are supported at each energy level in all cases of the bar's perturbation, namely, the envelope of the bar, the ring, and bar-driven spiral structures.

In the left column of Fig. 12, one can observe spiral structures that spread out at larger radii for the same time of integration as the bar's perturbation increases from $M_b = 9$ (20% in forces) to $M_b = 25$ (60% in forces). In fact, for $M_b = 9$ we observed that the apocentric sections support the envelope of the bar and a pseudo-ring structure of the R_1 type and then quickly become diffused outwards without supporting any prominent spiral structures. For larger values of the bar's perturbation, spiral structures are supported for increasingly larger distances.

In the middle column of Fig. 12, one can observe that the sticky chaotic orbits support the envelope of the bar and a

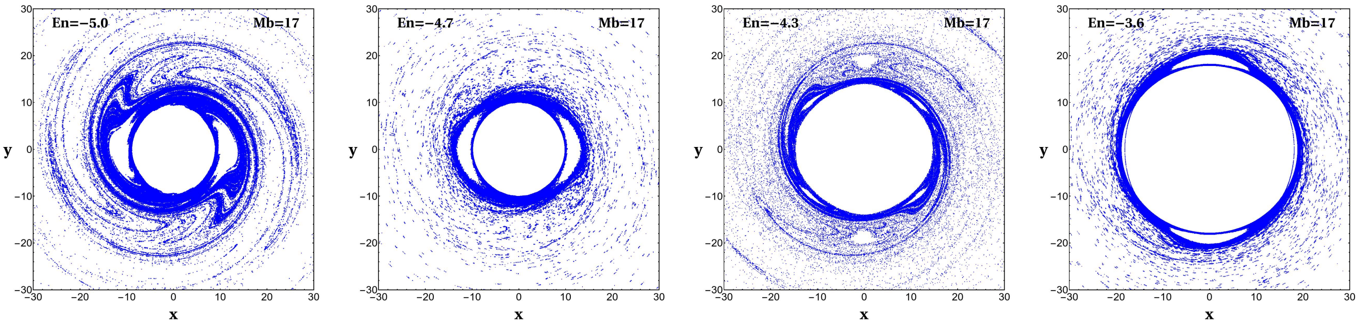

Fig. 11. Apocentric sections in the configuration space *x*-*y* of 3D sticky chaotic orbits outside corotation supporting different structures of the barred galaxy for different energies (En = −5, −4.7, −4.3, and −3.6) for M_b = 17. Spiral arms are supported for lower values of the energy (En), while the envelope of the bar and R_1- and R_2-type ring structures are supported for greater values of En.

pseudo-ring of the R_1 type for all the values of the bar's perturbation. Finally, in the right column of Fig. 12, a larger outer ring of the R_1 type is supported by the apocentric section of the orbits, where they reach larger distances for larger values of the parameter M_b. We conclude that the structures supported by apocentric sections exist for all the values of the bar's perturbation, but as the bar's perturbation increases, the radii at which the spiral structures extend also increase for the same time of integration.

In order to calculate the stickiness time (or escape time) of the 3D sticky chaotic orbits lying above the planar regular motion (see Fig. 8) for different initial z-components, we plotted the time evolution of the $FT - LCN$ for $M_b = 17$ and $En = -5.0$ (in Fig. 13a) and for $M_b = 25$ and $En = -5.0$ (in Fig. 13b). From the resulting figure, we observed that for initial conditions of the third dimension ($z_0 \leq 0.25$), all the sticky chaotic orbits behave as regular ones for times comparable to the Hubble time (vertical line) in both cases. On the other hand, in the case of the smallest bar's mass (M_b=17, Fig. 13a), we observed that most of the sticky chaotic orbits behave as regular ones and stay located inside the regular region of the galaxy for hundreds of Hubble times before expressing their chaotic behaviour and escaping from the system, while in the case of the larger bar's mass (M_b=25, Fig. 13b), the orbits escape much faster from the system. In general, we conclude that for all the values of the bar's perturbation, there are 3D sticky chaotic orbits that stay located inside or outside the region of regular motion and support the structures of the galaxy, but the stickiness time is increasingly longer as the bar's perturbation decreases.

4. Conclusions and discussion

We have studied a Milky Way-like barred galactic model where the free parameter is the bar's perturbation (mass of the bar, M_b, or perturbation in forces, Q_f) and tried to understand how the internal dynamics define the morphological structures supported in the configuration space of the galaxy. This paper is a continuation of Paper I, where we studied the case of a small bar perturbation ($Q_f \approx 12\%$). Here, we have studied models with bar perturbation values that range from $Q_f \approx 20\%$ to $Q_f \approx 60\%$ (see Fig. 1).

We located the planar orbits $PL_{1,2}$ for all the models and for different energy levels (En) and calculated their unstable manifolds in order to study the behaviour of the 3D sticky chaotic orbits lying along and above these planar manifolds in the 4D PSS ($y, \dot{y}, z, \dot{z}$, for x=0). Based on calculating the stability indices $b1, b2$ as a function of the energy (En) of the planar $PL_{1,2}$ orbits (for a bar perturbation of $M_b = 17$, or perturbation in forces of $Q_f = 40\%$), we conclude that there are, in general, several branches of the $PL_{1,2}$ family of orbits that coexist in some energy levels. With the help of the 4D PSS, we found 3D sticky chaotic orbits above planar unstable manifolds (with a small z component) outside the region of regular motion that remain located inside the galaxy for times comparable to the Hubble time. Using the method of apocentric sections, we then found the structures that are supported by these 3D sticky chaotic orbits for all the values of the bar's perturbation and for different energy levels.

The main conclusion is that contrary to the case of small bar perturbation ($Q_f \approx 12\%$, in Paper I), where the 3D sticky chaotic orbits support only ring or pseudo-ring-like structures (of the R_1 and R_1R_2' type), here as the bar's perturbation becomes greater and greater, bar-driven spiral structures are supported at greater and greater distances. At the same time, different structures can be supported at different energy levels in all cases of the bar's perturbation, including the envelope of the bar, outer ring structures of the R_1 type, and spiral arms.

We have shown that the 3D chaotic orbits that support the structures of the galaxy are sticky to some hypersurfaces in the 4D PSS outside the SZV. These hypersurfaces that could be some 3D manifolds in the 4D PSS are the subject of a future study.

Furthermore, there are 3D sticky chaotic orbits that behave for a very long time (compared to the Hubble time) as regular orbits and then become diffused inwards towards the centre of the galaxy before finally escaping from the system. The stickiness time (or escape time) of these orbits can be found by calculating the time evolution of the $FT - LCN$, which shows the stickiness phenomena for hundreds of Hubble time.

The results of this paper as well as of Paper I are in agreement with many observational studies that calculate the bar-induced perturbation strengths of barred spiral galaxies using the force perturbation (Q_f). Studies such as Block et al. 2004, Laurikainen et al. 2004, Buta et al. 2005, and Buta et al. 2009, show that in general, barred galaxies with a smaller force perturbation often present ring-like structures, while others with a greater Q_f present bar-driven spiral arms. Similar results have also been found in studies of 2D models of barred galaxies (Romero-Gómez et al. 2007).

There are also studies that have concluded a weak correlation between the strength of the bar and the strength of the spiral arms. These correlations suggest that the bars and spirals grow together with the same rates and pattern speeds (Block et al. 2004; Athanassoula et al. 2009). In our study, we observed this correlation, but we did not investigate the implications of a different pattern speed of the bar (Ω_b) or of a distinct spiral poten-

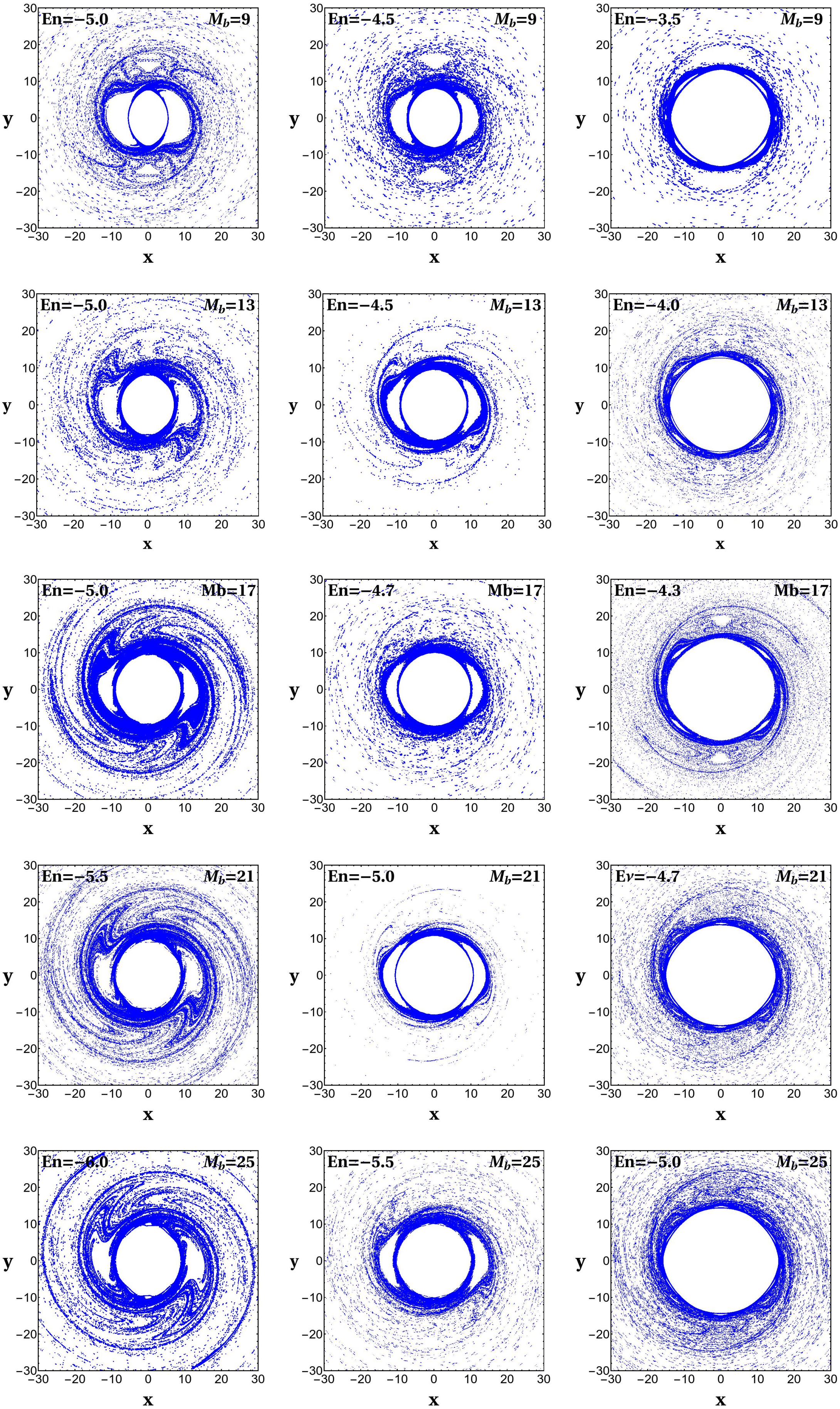

Fig. 12. Apocentric sections on the configuration space x-y of 3D sticky chaotic orbits outside corotation supporting different structures of the barred galaxy for different energies. Each row corresponds to a model with the same bar perturbation, from M_b = 9 at the top to M_b = 25 at the bottom. The spiral arms are more enhanced and extend over greater distances for greater values of M_b. Depending on the energy level, the envelope of the bar as well as outer ring structures of the R_1 type are supported.

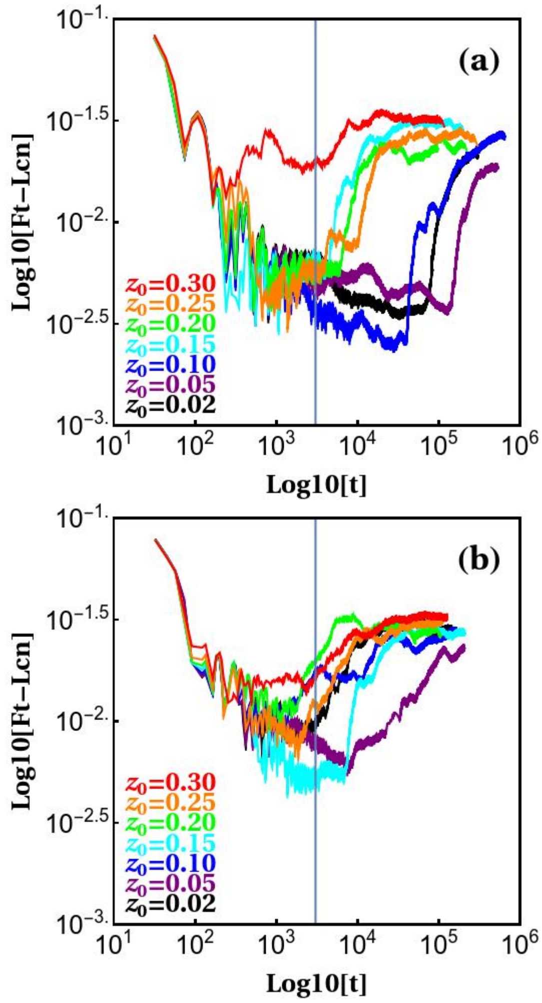

Fig. 13. Time evolution of the $FT - LCN$ of 3D sticky chaotic orbits for (a) $M_b = 17$ and $En = -5.0$ and (b) $M_b = 25$ and $En = -5.0$ for different values of the initial z component.

tial on the galactic structures in the configuration space. These questions remain open, and we aim to answer them in our future work.

Finally, we wish to point out that although real barred galaxies have time-dependent potentials, the study of an autonomous steady state galactic model can be used as a dynamical laboratory that allows one to determine where the sticky zones are, how escape occurs, and the distribution of escape times during which chaotic orbits support rings and spirals. These are intrinsic properties of the Hamiltonian phase space. Although during the slowdown of the bar in a real barred galaxy the Lagrangian points $L_{1,2}$ move outwards together with corotation and the position of the periodic orbits $PL_{1,2}$ change continuously, the hypersurfaces network of the 4D PSS often persists and deforms adiabatically rather than disappearing abruptly. Hence, the autonomous manifolds and hypersurfaces that are responsible for the stickiness of chaotic orbits reveal the underlying pattern that the evolving galaxy follows. In real non-autonomous barred galaxies, sticky chaotic orbits near corotation may escape after some long timescale, but they are replenished by other stars that pass through the dynamical channels associated with the Lagrangian points. In Voglis et al. 2006b, the authors showed in their N-body simulations that spiral arms are spontaneously formed on the disc and show an intermittent behaviour as they are deformed, fade, or disappear temporarily, but they grow again in a timescale less than the rotation period of the bar. The m = 2 mode preserves its spiral structure outside corotation for a Hubble time, during which the bar describes about 20-30 rotations. Therefore observed spiral arms and rings may be maintained by a flux of chaotic orbits rather than by the long-term trapping of a fixed population. A barred galaxy evolves on secular timescales of roughly 1–10 billion years, i.e. a significant fraction of a Hubble time. However, this is much slower than orbital motion but not negligible compared with long chaotic trapping times. If sticky times are comparable to or longer than the bar evolution time, then manifold-supported spirals and rings can remain morphologically persistent even though individual stars are continuously replaced. In that sense, the non-autonomous galaxy continuously repopulates manifold-supported spirals and rings as the bar slows, and corotation migrates through the dynamical channels associated with the Lagrangian points.

Acknowledgements. We would like to thank Prof. G. Contopoulos for fruitful discussions and very useful comments. This work was funded by the Sectoral Development Program ("ΟΠΣ" 5223471) of the Ministry of Education, Religious Affairs and Sports, through the National Development Program (NDP) 2021-25. It was conducted as part of project 200/1022, supported by the Research Committee of the Academy of Athens.

References

Agaoglou M., García-Garrido, V. J., Katsanikas, M. and Wiggins S., Comm. Nonlin. Sci. Num. Sim., 103, 105993, 2021
Athanassoula E. and Misiriotis A., MNRAS, 330, 35, 2002
Athanassoula E., Romero-Gómez M., Bosma A., Masdemont J. J., MNRAS, 400, 1706, 2009
Block D. L., Buta R., Knapen J. H., Elmegreen D. M., Elmegreen B.G. and Puerari I, Astron. J., 128, 183, 2004
Joss Bland-Hawthorn J. and Gerhard O., Annu. Rev. Astron. Astrophys., 54, 529, 2016
Buta R. and Combes F., Fund. Cosmic Physics, 17, 95, 1996
Buta R., Vasylyev S., Salo H. and Laurikainen E., Astron. J., 130, 506, 2005
Buta R., Knapen J., Elmegreen B, Salo H., Laurikainen E., Elmegreen D., Puerari I. and Block D., Astron. J., 137, 4487, 2009
Chaves-Velasquez L., Patsis P. A., Puerari I., Skokos Ch. and Manos T., ApJ, 850, 145, 2017
Cincotta P.M. and Simó C., Astron. Astrophys. Suppl. Ser. 147, 205, 2000
Cincotta P.M. and Giordano C.M., MNRAS, 526, 895, 2023
Contopoulos G. and Papayannopoulos T., Astron. Astrophys, 92, 33, 1980
Contopoulos G. and Harsoula M., IJBC, 18, 2929, 2008
Contopoulos G. and Harsoula M., CeMDA, 107, 77, 2010a
Contopoulos G. and Harsoula M., IJBC, 20, 2005, 2010b
Contopoulos G. and Harsoula M., MNRAS, 436, 1201, 2013
Gadotti D. A., MNRAS, 415, 3308, 2011
Gerhard O., Memorie della Societa Astronomica Italiana Sup, 18, 185, 2011
Froeschlé C., Lega E. and Gonczi R., CeMDA, 67, 41, 1997
Géron T., Smethurst R.J., Lintott Ch., Kruk S., Masters K.L., Simmons B., Mantha K.B., Walmsley. M., Garma-Oehmichen L., Drory N. and Lane R.R, MNRAS, 521, 1775, 2023
Guo R., Mao Sh., Athanassoula E., Li H., Ge J., Long R. J., Merrifield M., Masters K., MNRAS, 482, 1733, 2019
Harsoula M. and Katsanikas M., Astron. Astrophys., 699, 16, 2025 (Paper I)
Katsanikas M. and Patsis, P.A., Int. J. Bif. Ch., 21, 467, 2011
Katsanikas M., Patsis P. A. and Contopoulos G., IJBC, 21, 2321, 2011a
Katsanikas M., Patsis P. A. and Pinotsis A. D., IJBC, 21, 2331, 2011b
Katsanikas M., Patsis, P. A. and Contopoulos, G., IJBC, 23, 1330005, 2013
Katsanikas M. and Patsis, P.A., MNRAS, 516, 5232, 2022
Kaufmann D.E. and Contopoulos G., Astron. Astrophys., 309, 381, 1996
Laurikainen E., Salo H., Buta R. and Vasylyev S., MNRAS, 355, 1251, 2004
Long K. and Murali C., ApJ, 397, 44L, 1992
Mengistu P., Masters K.L., Géron T., Smethurst R.J., Lintott Ch. and Simmons B.D., MNRAS, 548, 1, 2026
Moges H. T., Katsanikas M., Patsis P. A., Hillebrand M. and Skokos Ch., IJBC, 34, 30013, 2024
Morbidelli A. and Giorgilli A., JPS, 78, 1607, 1995
Patsis P. A. and Zachilas L., Int. J. Bif. Chao., 04, 1399, 1994
Patsis P.A., Skokos Ch. and Athanassoula E., MNRAS, 346, 1031, 2003
Patsis P.A., Kaufmann D.E., Gottesman T. and Boonyasait V., MNRAS, 394, 142, 2009
Patsis P. A. and Katsanikas M., MNRAS, 445, 3525, 2014
Perry A. and Wiggins S., Physica D, 71, 102, 1994
Rautiainen P., Salo H. and Laurikainen E., MNRAS, 388, 1803, 2008
Romero-Gómez M., Masdemont J. J. and Athanassoula E., Astron. Astrophys., 453, 39, 2006
Romero-Gómez M., Athanassoula E. and Masdemont J. J., Astron. Astrophys., 472, 63, 2007
Sanders J. L., Smith L. and Evans N. W., MNRAS, 488, 4552S, 2019
Sierra A.D., Seigar M.S., Treuthardt P. and Puerari I., MNRAS, 450, 1799, 2015
Skokos, C., J.Phys. A., 34, 10029, 2001
Skokos C., Bountis T. C. and Antonopoulos C., Phys. D.,31, 30, 2007
. Smith R., Flynn, C., Candlish G. N., Fellhauer M. and Gibson B. K., MNRAS, 448, 3, 2934, 2015
Tsallis C., Jour.Stat. Phys., 52, 479, 1988
Tsoutsis P., Efthymiopoulos C. and Voglis N., Mon. Not. R. Astron. Soc., 387, 1264, 2008
Tsoutsis P., Kalapotharakos C., Efthymiopoulos C. and Contopoulos G., Astron. and Astrophys., 495, 743, 2009
Voglis N., Tsoutsis P. and C. Efthymiopoulos, Mon. Not. R. Astron. Soc., 373, 280, 2006
Voglis N., Stavropoulos I. and Kalapotharakos C., MNRAS, 372, 901, 2006b
Zachilas L., Katsanikas M. and Patsis P. A., IJBC, 23, 1330023, 2013
Wiggins S., Garcia-Garrido V. J. and Katsanikas, M., "Phase Space Structures in Reaction Dynamics: A Dynamical Systems Approach", World Scientific, ISBN: 978-981-98-1539-5, 2025.